Research in Pharmaceutical Sciences, December 2025; 20(6): 853-865
Received: 08-04-2025
Peer Reviewed:10-05-2025
Revised: 07-06-2025
Accepted: 08-06-2025
Published: 15-11-2025

School of Pharmacy & Pharmaceutical Sciences
Isfahan University of Medical Sciences

Original Article

Sulforaphane attenuates oxidative stress, senescence, and ferroptosis induced by cigarette smoke extract *in vitro* and *in vivo via* upregulating the expression of SIRT1

Amin Reihani[1,2], Ebrahim Mohammadi[3], Fereshteh Talebpour Amiri[4], Mohammad Seyedabadi[2,*], and Fatemeh Shaki[2,*]

[1]*Student Research Committee, Faculty of Pharmacy, Mazandaran University of Medical Sciences, Sari, Iran.*
[2]*Department of Toxicology and Pharmacology, Faculty of Pharmacy, Mazandaran University of Medical Sciences, Sari, Iran.*
[3]*Environmental Health Research Center, Research Institute for Health Development, Kurdistan University of Medical Sciences, Sanandaj, Iran.*
[4]*Department of Anatomy, Faculty of Medicine, Molecular and Cell Biology Research Center, Mazandaran University of Medical Sciences, Sari, Iran.*

Abstract

Background and purpose: Cigarette smoking induces lung toxicity by triggering oxidative stress, leading to apoptosis, ferroptosis, and senescence. Sulforaphane (SFN), a potent antioxidant, activates the SIRT1 pathway, enhancing cellular stress resistance and survival. This study aimed to evaluate the protective effects of SFN against cigarette smoke extract (CSE)-induced damage in human airway epithelial cells (BEAS-2B) and in mouse lungs, focusing on its role in upregulating SIRT1 expression.

Experimental approach: BEAS-2B cells were treated with CSE and SFN, and cell viability was assessed using the MTT assay. Cellular senescence was assessed using the SA-β-gal assay and the expression of genes associated with senescence (p16 and p21). The expression levels of SIRT1, senescence-associated secretory phenotype (SASP) cytokines (IL-1β, IL-6, IL-8, TNF-α), GPX4, and SLC7A11 were quantified using qRT-PCR. Additionally, ROS production, GSH and MDA levels, and iron content were measured. An emphysema mouse model was induced by intraperitoneal administration of CSE (7.2 mg/kg) alone or in combination with SFN (10.2 mg/kg) over 28 days, and subsequent histopathological changes were evaluated.

Findings/Results: Our findings revealed that SFN co-treatment effectively mitigated CSE-induced cytotoxicity, senescence, and SASP cytokine secretion, as well as the pronounced emphysematous changes in lung tissues. Furthermore, SFN reversed CSE-induced downregulation of SIRT1 and upregulation of NF-κB. Notably, SFN also inhibited CSE-induced ferroptosis by increasing GPX4 and SLC7A11 expression while reducing iron and MDA levels.

Conclusion and implications: The findings of the present study demonstrated that sulforaphane offers protective effects against CSE-induced toxicity by mitigating oxidative stress, ferroptosis, and cellular senescence.

Keywords: Cellular senescence; Cigarette smoke extract; Ferroptosis; SIRT1; Sulforaphane.

INTRODUCTION

Cigarette smoke (CS) is a complex aerosol comprised of thousands of chemical compounds, many of which have demonstrated deleterious effects on various cellular functions and signaling pathways (1). CS is the most extensively documented and significant risk factor for the development and progression of chronic obstructive pulmonary disease (COPD) (2).

*Corresponding authors:
F. Shaki, Tel: +98-1133543081-3; Fax: +98-1133543084
Email: fshakki@mazums.ac.ir
M. Seyedabadi, Tel: +98-1133543081-3; Fax: +98-1133543084
Email: m.seyedabai@mazums.ac.ir

Access this article online	
	Website: http://rps.mui.ac.ir
	DOI: 10.4103/RPS.RPS_55_25

COPD is characterized by persistent airway obstruction and chronic inflammation within the pulmonary system, contributing to the development of emphysema and chronic bronchitis (3). Each puff of CS contains approximately 10^{15}-10^{17} oxidative free radicals (4). Oxidative stress, marked by elevated intracellular levels of reactive oxygen species (ROS), leads to damage to essential biomolecules such as DNA, proteins, and lipids (5). CS has long been recognized as a key factor in the premature aging of the lungs, primarily due to the direct exposure of pulmonary tissues to oxidants and free radicals from inhaled cigarette smoke (6).

COPD is closely associated with the accelerated aging of pulmonary tissues (7). A hallmark of the aging process is cellular senescence, a state defined by permanent withdrawal from the cell cycle and accompanied by morphological and functional alterations (8). Senescent cells can be identified by the expression of senescence-associated biomarkers such as p16, p21, and senescence-associated β-galactosidase (SA-β-gal). In addition to their impaired proliferative capacity, senescent cells exhibit a distinct secretory profile known as the senescence-associated secretory phenotype (SASP), characterized by the excessive release of pro-inflammatory cytokines, chemokines, growth factors, and proteases (9). The SASP can have deleterious effects on the tissue microenvironment, potentially exacerbating pathological conditions by impairing the function and viability of neighboring cells (10,11). In COPD, CS has been recognized as a major contributor to the induction of cellular senescence (12).

Ferroptosis is a form of regulated cell death that is iron-dependent and non-apoptotic. It is induced by the generation of hydroxyl radicals through the Fenton reaction, in which ferrous iron (Fe^{2+}) reacts with peroxides, leading to oxidative damage and cell death (13). Ferroptosis is characterized by dysregulation of iron metabolism, excessive accumulation of ROS, depletion of glutathione (GSH), and inactivation of glutathione peroxidase 4 (GPX4) (14-16). Previous studies have further indicated that exposure to CS induces ferroptotic cell death in human bronchial epithelial (BEAS-2B) cells. (17). Sirtuins are conserved NAD(+)-dependent deacetylases essential for promoting metabolism and longevity (3). In mammals, there are seven sirtuins (SIRT1-7) (18). Research has demonstrated that silent information regulator 1 (SIRT1) plays a crucial role in protecting against cellular senescence and inflammation by regulating various cellular processes (19,20). SIRT1 removes acetyl groups from multiple target genes, including the nuclear factor kappaB (NF-κB), thereby regulating their activities (21). NF-κB is a crucial transcription factor activated in numerous diseases associated with the SASP (3). SIRT1 also plays a critical role in modulating cellular metabolism and promoting longevity by regulating stress responses, inflammation, and mitochondrial function; its decline has been implicated in age-related diseases, including COPD (22,23).

Sulforaphane (SFN), a bioactive isothiocyanate, originates from the enzymatic hydrolysis of glucoraphanin, a precursor compound prevalent in cruciferous vegetables like broccoli and Brussels sprouts (24). A considerable body of research has established that SFN, owing to its antioxidant characteristics, has the potential to activate phase II detoxification enzymes (25,26). Considering the antioxidant and anti-inflammatory properties of SFN, along with the well-documented association between smoking and COPD through mechanisms such as oxidative stress, senescence, and ferroptosis, we propose that SFN may offer a protective effect by modulating these pathological processes. Therefore, the main aim of this study was to investigate the protective effects of SFN against CSE-induced oxidative stress, cellular senescence, and ferroptosis. We further aimed to elucidate the underlying molecular mechanisms, with a specific focus on the modulation of the SIRT1 signaling pathway. These objectives were addressed through both *in vitro* and *in vivo* models, using bronchial epithelial cells and a mouse model of CSE exposure, respectively.

MATERIALS AND METHODS

Reagents and chemicals

In this investigation, SFN (Sigma-Aldrich, USA, purity ≥ 98%) was utilized after being diluted in 10% dimethyl sulfoxide (DMSO), maintaining a final DMSO concentration of no more than 0.1%. Culture media and supplements, including Roswell Park Memorial

Institute (RPMI) 1640 and fetal bovine serum (FBS), were procured from DNAbiotech (Iran). CSE (40 mg/mL in DMSO) was acquired from the Kentucky Tobacco Research and Development Center, derived from the standardized Kentucky reference cigarette (1R6F). Deferoxamine (DFO) was supplied by Samen (Iran), while dichlorodihydrofluorescein diacetate (DCFH-DA) was obtained from Merck Co. (Germany).

Preparation of CSE

Commercially prepared CSE was obtained from the Kentucky Tobacco Research and Development Center. The CSE was derived from standardized 1R6F and provided as a concentrated stock solution at a concentration of 40 mg/mL in DMSO. Upon receipt, the CSE was transported on dry ice and stored at -80 °C in sterile, light-protected microcentrifuge tubes until use. Before each experiment, aliquots of the stock solution were freshly thawed and diluted with RPMI-1640 medium to achieve final concentrations ranging from 0.01 to 100 µg/mL. All handling and dilution procedures were performed under aseptic conditions and protected from light to preserve the chemical stability and sterility of the extract.

Cell treatment

BEAS-2B human bronchial epithelial cells (Pasteur Institute, Iran) were grown in RPMI medium enriched with 10% FBS, 100 µg/mL penicillin, 100 U/mL streptomycin, and 5 mM L-glutamine. Cells were cultured at 37 °C in a humidified incubator with 7.5% CO_2. The experimental design consisted of six treatment groups, including the control group: cells maintained under standard conditions; SFN group: cells exposed to the highest non-toxic SFN concentration (20 µg/mL) to evaluate SFN's standalone effects; CSE group: cells treated with the half-maximal drug inhibitory concentration (IC_{50}) of CSE (59.5 µg/mL) for 24 h; CSE + SFN: co-treatment with CSE (59.5 µg/mL) and low (5 µg/mL), medium (10 µg/mL), or high (20 µg/mL) concentrations of SFN.

All treatments were administered for 24 h under standard culture conditions. This model was designed to evaluate the protective or modulatory effects of SFN against CSE-induced cellular stress in a concentration-dependent manner.

Animal

A murine model of emphysema was established based on a previously published protocol (27). Twenty-four male mice (6 weeks old, 21-23 g) were randomly divided into three groups (n = 8 each), including group A (control): received intraperitoneal (i.p.) injections of phosphate-buffered saline (PBS, 0.3 mL) on days 0, 11, and 22; group B (CSE): administered CSE *via* i.p. injection at a dosage of 7.2 mg/kg on the same days; group C (CSE + SFN): received combined i.p. injections of CSE (7.2 mg/kg) and SFN (10.2 mg/kg) on days 0, 11, and 22. Animals were euthanized on day 28. All procedures complied with the ethical standards set by the MASUMS Ethics Committee (Ethic code: IR.MAZUMS.AEC.1403.043).

MTT assay

To assess cytotoxicity, BEAS-2B cells were seeded at a density of 4×10^4 cells per well in 48-well plates and allowed to adhere overnight. Cells were then treated with varying concentrations of CSE (0.01-100 µg/mL), SFN (0.01-50 µg/mL), or co-treatment with both agents for 24 h. After treatment, the culture medium was removed, and cells were gently rinsed with PBS to eliminate residual treatment compounds. Subsequently, 50 µL of MTT solution (0.5 mg/mL) was added to each well, and cells were incubated for 3 h at 37 °C. The resulting formazan crystals were dissolved in 170 µL of DMSO, and absorbance was measured at 570 nm using a microplate reader (28). Cell viability was expressed as a percentage relative to untreated controls.

ROS production evaluation

BEAS-2B cells were seeded in 6-well plates at a density of 2×10^5 cells per well and allowed to adhere overnight in RPMI medium supplemented with 10% FBS. The next day, cells were treated with CSE, SFN, or their combination for 24 h, depending on the experimental group. Following treatment, cells were harvested by trypsinization and washed twice with PBS. DCFH-DA (10 µmol/L) was added to each well, followed by 30 min of incubation at 37 °C. The cells were homogenized and centrifuged at 10,000 *g* for 5 min. Supernatants (200 µL) were analyzed using a spectrofluorometer at 485 nm excitation

and 535 nm emission wavelengths (29). Fluorescent intensity values were normalized to the cell number.

GSH and MDA quantification

BEAS-2B cells were seeded in 6-well plates at a density of 2×10^5 cells per well and allowed to adhere overnight in RPMI medium supplemented with 10% FBS. The next day, cells were treated with CSE, SFN, or their combination for 24 h, depending on the experimental group. Following treatment, cells were harvested by trypsinization and washed twice with PBS. For GSH analysis, cell lysates prepared in Triton-X-100 buffer were centrifuged, and supernatants were reacted with DTNB (200 µM) for 30 min. Absorbance was measured at 405 nm. For MDA assessment, lysates were reacted with 0.2 M phosphoric acid and 0.6% thiobarbituric acid (TBA), incubated at 100 °C, cooled, extracted with n-butanol, and centrifuged. The upper phase absorbance was read at 532 nm, allowing for lipid peroxidation analysis.

SA-β-gal activity

BEAS-2B cells were seeded in 6-well plates at a density of 2×10^5 cells per well and allowed to adhere overnight in RPMI medium supplemented with 10% FBS. The next day, cells were treated with CSE, SFN, or their combination for 24 h, depending on the experimental group. Following treatment, cells were harvested by trypsinization and washed twice with PBS. SA-β-gal activity was determined using a colorimetric assay involving o-nitrophenyl-β-D-galactopyranoside (ONPG) as a substrate (30). Upon enzymatic hydrolysis, ONPG releases a yellow product (o-nitrophenol), which was quantified at 420 nm in alkaline conditions (pH 10.2). Results were normalized to cell count.

Intracellular iron determination

BEAS-2B cells were seeded in 6-well plates at a density of 2×10^5 cells per well and allowed to adhere overnight in RPMI medium supplemented with 10% FBS. The next day, cells were treated with CSE, SFN, or their combination for 24 h, depending on the experimental group. Following treatment, cells were harvested by trypsinization and washed twice with PBS. Intracellular iron was quantified with the Agilent 4210 microwave plasma atomic emission spectroscopy (MP-AES) instrument. Cells were incubated in a mixture of 0.1% nitric acid and 0.1% Triton X-100 at 60 °C for 14 h (31). The solution was then preserved in 0.2 M nitric acid until elemental analysis was performed.

Quantitative real-time polymerase chain reaction

Total RNA was isolated using TrizoLEX reagent (DNAbiotech, Iran), and RNA purity and concentration were assessed *via* absorbance at 260 and 280 nm using a Nanodrop spectrophotometer. Complementary DNA (cDNA) was synthesized from 1 µg of total RNA using the Easy cDNA Ultra-TM synthesis kit (Parstous, Iran) according to the manufacturer's instructions. Quantitative real-time polymerase chain reaction (qRT-PCR) was performed using SYBR Green master mix (Zistviraiesh, Iran) on an Mx3000P real-time PCR system (Agilent Technologies, USA). Gene-specific primers were designed using Primer-BLAST (NCBI) and synthesized by Metabion (Germany). The sequences of all primers used are listed in Table 1. Each qRT-PCR reaction was carried out in a 20 µL volume containing 10 µL SYBR Green master mix, 0.5 µL of each primer (10 µM), 2 µL of cDNA, and 7 µL nuclease-free water.

Thermal cycling conditions were as follows: initial denaturation at 95 °C for 10 min, followed by 40 cycles of denaturation at 95 °C for 15 s, annealing at 60 °C for 30 s, and extension at 72 °C for 30 s. Melt curve analysis was performed to verify the specificity of the amplification. Relative gene expression levels were calculated using the $2^{-\Delta\Delta Cq}$ method, with GAPDH used as the internal control (32).

Histopathologic analysis

Lung tissues were fixed in 10% formalin, sectioned into 5-µm slices, and stained using hematoxylin and eosin (H&E). Histopathological evaluations were performed microscopically to detect structural changes associated with treatment conditions. In addition, a blinded morphometric analysis of alveolar airspace enlargement was conducted using the mean linear intercept (MLI) method to provide semi-quantitative confirmation of the observed changes.

Table 1. Primer sequences.

Gene	Primer sequence (5′–3′)	
SIRT1	Forward: GGAGCAGATTAGTAAGCGGCTTG	Reverse: GTTACTGCCACAGGAACTAGAGG
NF-κB	Forward: TACGGATTCTGGTGGGGTGT	Reverse: CCATCAGGACAGGGGAAAAGT
P16	Forward: CTCTGAGAAACCTCGGGAAACT	Reverse: AACTACGAAAGCGGGGTGG
TNF-α	Forward: CTCTTCTGCCTGCTGCACTTTG	Reverse: RTGGGCTACRGGCTTGTCACTC
IL-6	Forward: CCGGAGAGGAGACTTCACAGC	Reverse: AGATTGCCATTGCACACC
IL-8	Forward: AGAACATCCAGAGTTTGAAGGTGAT	Reverse: GTGGCTATGACTTCGGTTTGG
Il-1β	Forward: TCCCCAGCCCTTTTGTTGA	Reverse: TTAGAACCAAATGTGGCCGTG
SLC7A11	Forward: TCCTGCTTTGGCTCCATGAACG	Reverse: AGAGGAGTGTGCTTGCGGACAT
GPX4	Forward: ACAAGAACGGCTGCGTGGTGAA	Reverse: GCCACACACTTGTGGAGCTAGA
P21	Forward: TTCCTCATCCACCCCATCC	Reverse: CCCTGTCCATAGCCTCTACTGC
GAPDH	Forward: GCACCGTCAAGGCTGAGAAC	Reverse: TGGTGAAGACGCCAGTGGA

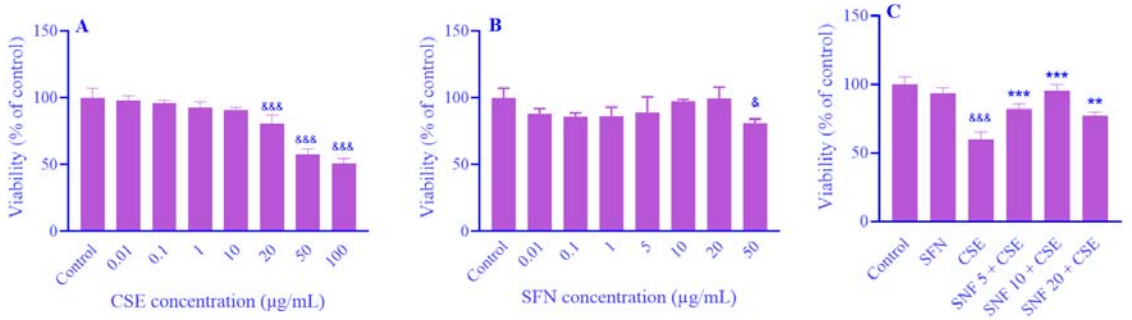

Fig. 1. The effect of (A) CSE, (B) SFN, and (C) the combination treatment of SFN (5, 10, and 20 μg/mL) with 59 μg/mL CSE on BEAS-2B cell viability. The data are expressed as mean ± SD. $^{\&}P < 0.05$ and $^{\&\&\&}P < 0.001$ indicate significant differences compared to the control group; $^{**}P < 0.01$ and $^{***}P < 0.001$ versus CSE group. SFN, Sulforaphane; CSE; cigarette smoke extract.

Statistical analysis

GraphPad Prism version 8.4.2 (Dotmatics) was used for all data analyses. Results are reported as mean ± SD from at least three independent experiments. Statistical significance among groups was evaluated using one-way ANOVA followed by Tukey's post hoc test. P-values < 0.05 were considered statistically significant.

RESULTS

Impact of CSE, SFN, and their combination on BEAS-2B cell viability

To evaluate how CSE, SFN, and their combined use affect BEAS-2B cell survival, MTT assays were conducted. Significant cytotoxicity was observed with CSE at concentrations of 20, 50, and 100 μg/mL, and the IC_{50} was calculated to be 59 μg/mL (Fig. 1A). SFN induced cytotoxic effects at 50 μg/mL following 24 h of treatment (Fig. 1B). For co-treatment experiments, the IC_{50} concentration of CSE was used in conjunction with three SFN doses (5, 10, and 20 μg/mL) to examine potential synergistic effects (Fig. 1 C).

SFN prevents oxidative stress in BEAS-2B

This study aimed to determine whether SFN could counteract oxidative damage caused by CSE. Cellular GSH and ROS levels were measured post-treatment. Exposure to CSE significantly increased ROS generation while depleting intracellular GSH. Treatment with SFN counteracted these effects, restoring GSH and reducing ROS levels, as depicted in Fig. 2A and B.

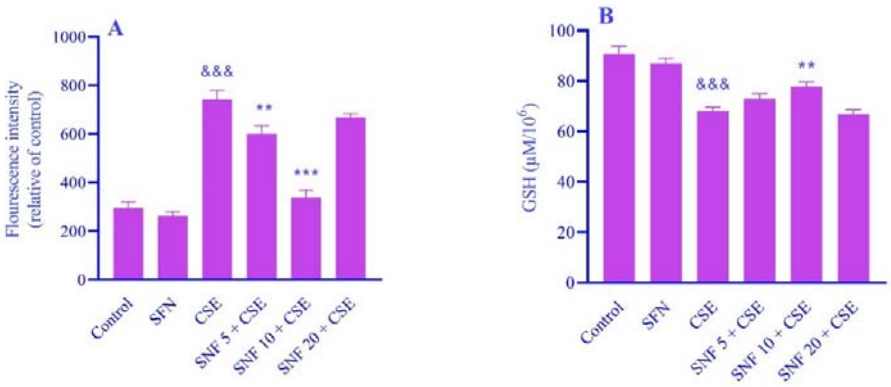

Fig. 2. Effects of SFN and CSE combination on stress oxidative in BEAS-2B cells. (A) Co-treating with SFN decreased the production of reactive oxygen species triggered by CSE. (B) GSH levels were measured based on the material and methods. The data are expressed as mean ± SD. $^{\&\&\&}P < 0.001$ indicates significant differences compared to the control group; $^{**}P < 0.01$ and $^{***}P < 0.001$ versus CSE group. SFN, Sulforaphane; CSE; cigarette smoke extract; GSH, glutathione

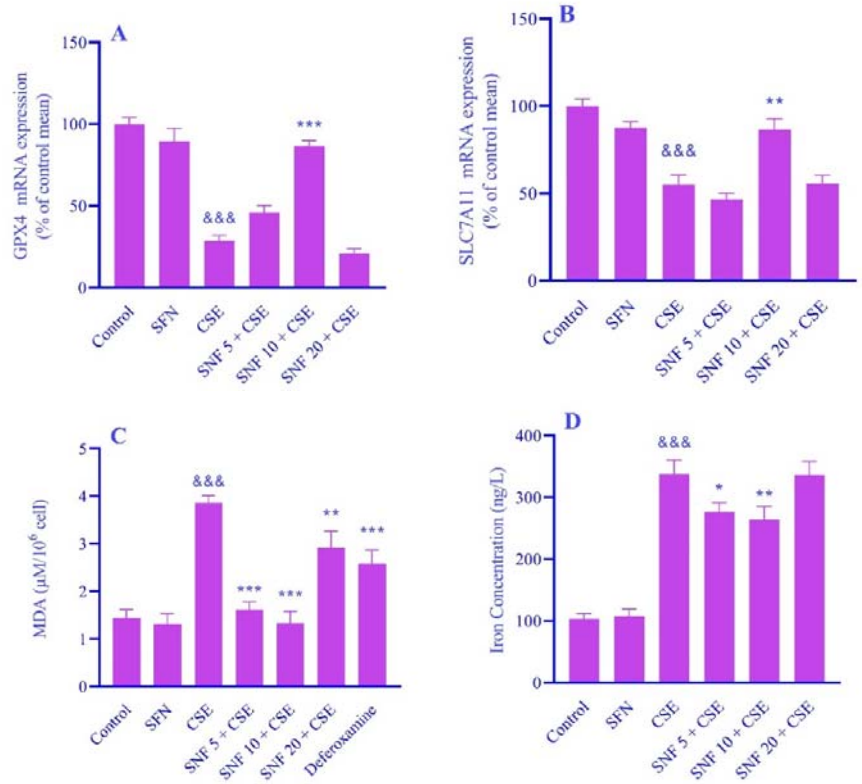

Fig. 3. Effects of SFN and CSE on ferroptosis. (A and B) qRT-PCR was used to analyze the mRNA level of GPX4 and SLC7A11. GAPDH was used for internal normalizations. (C and D) MDA and intracellular iron levels were measured in BEAS-2B cells. The data are expressed as mean ± SD. $^{\&\&}P < 0.01$ and $^{\&\&\&}P < 0.001$ indicate significant differences compared to the control group; $^{*}P < 0.05$, $^{**}P < 0.01$, and $^{***}P < 0.001$ versus CSE group. SFN, Sulforaphane; DFO, deferoxamine (10 mM); CSE, cigarette smoke extract; MDA, malondialdehyde; qRT-PCR, quantitative real-time polymerase chain reaction; GAPDH, glyceraldehyde-3-phosphate dehydrogenase.

SFN alleviates ferroptosis in CSE-treated cells

To understand SFN's role in modulating ferroptosis, mRNA levels of solute carrier family 7A member 11 (SLC7A11) and glutathione GPX4, key genes regulating this cell death pathway, were assessed using qRT-PCR. In addition, iron accumulation and lipid peroxidation, hallmarks of ferroptosis, were measured. The CSE-treated group exhibited downregulation of GPX4 and SLC7A11 (Fig. 3A and B), along with elevated MDA levels and intracellular iron content (Fig. 3C and D). These pro-ferroptotic changes were significantly mitigated following SFN treatment.

SFN attenuates CSE-induced cellular senescence

SA-β-gal activity was used to assess cellular aging. CSE exposure resulted in a marked increase in SA-β-gal activity (0.3395 ± 0.01) compared to untreated controls (0.07 ± 0.01). SFN administration at 10 μg/mL significantly lowered this activity (0.27 ± 0.02), as illustrated in Fig. 4A. Furthermore, CSE upregulated the mRNA expression of senescence markers p16 and p21, whereas SFN co-treatment reduced their expression (Fig. 4B and C), indicating that SFN can modulate senescence-related signaling pathways.

SFN reverses CSE-induced dysregulation of SIRT1, NF-κB, and SASP cytokines

qRT-PCR analysis was performed to evaluate the effects of CSE on the expression of SIRT1, NF-κB, and SASP cytokines (interleukin-1β (IL-1β), IL-6, IL-8), and tumor necrosis factor alpha (TNF-α)) in BEAS-2B cells. The results indicated a significant reduction in SIRT1 expression, along with a marked increase in NF-κB, TNF-α, IL-1β, IL-8, and IL-6 expression in the CSE-treated group compared to the control (Fig. 5A-F). Notably, SFN treatment effectively reversed the CSE-induced downregulation of SIRT1 and the upregulation of NF-κB and SASP cytokines, suggesting its potential protective role against CSE-induced inflammatory and senescence-associated responses (Fig. 5).

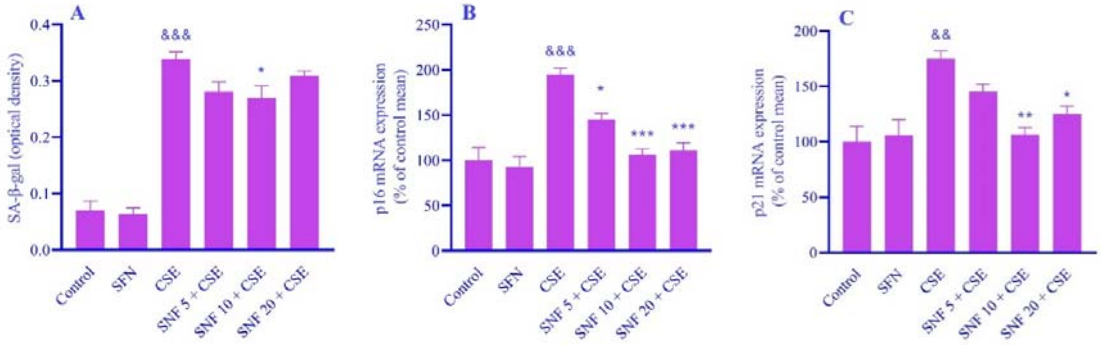

Fig. 4. The impact of SFN and CSE on senescence-related markers in BEAS-2B cells. (A) SA-β-gal activity was determined using a colorimetric assay. (B and C) qRT-PCR was used to analyze the mRNA levels of p16 and p21. GAPDH was used for internal normalizations. The data are expressed as mean ± SD. $^{\&\&}P < 0.01$ and $^{\&\&\&}P < 0.001$ indicate significant differences compared to the control group; $^{*}P < 0.05$, $^{**}P < 0.01$, and $^{***}P < 0.001$ versus CSE group. SFN, Sulforaphane; CSE, cigarette smoke extract; qRT-PCR, quantitative real-time polymerase chain reaction; GAPDH, glyceraldehyde-3-phosphate dehydrogenase.

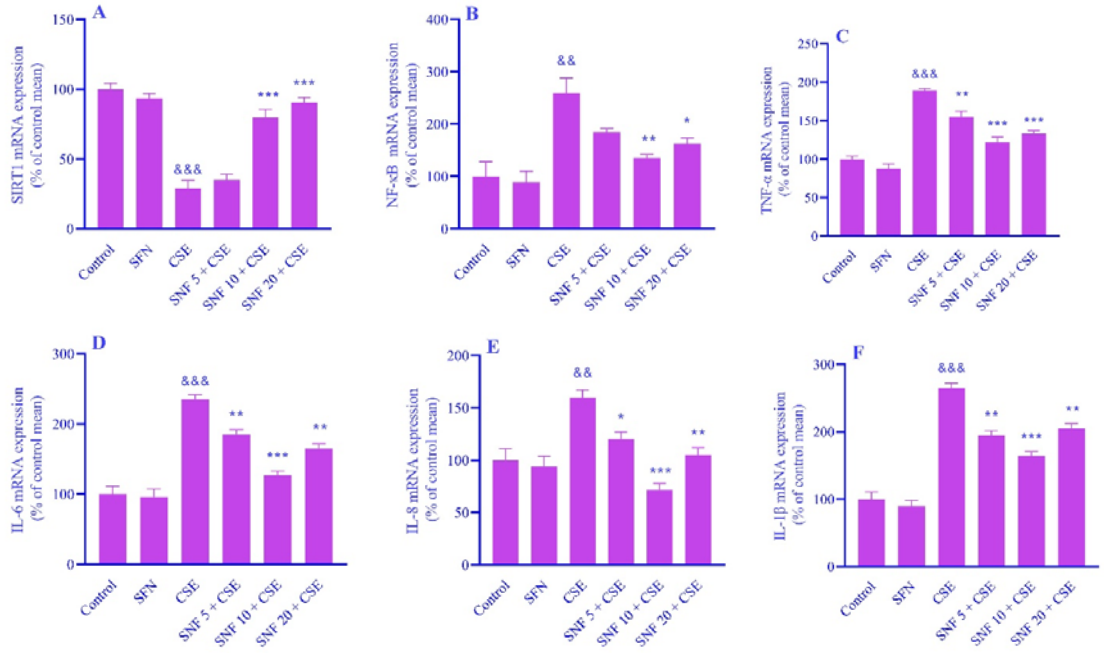

Fig. 5. Expression of (A) SIRT1, (B) NF-κB, (C) TNF-α, (D) IL-6, (E) IL-8, and (F) IL-1β in BEAS-2B cells. qRT-PCR was used to analyze mRNA expression. GAPDH was used for internal normalizations. The data are expressed as mean ± SD. $^{\&\&}P < 0.01$ and $^{\&\&\&}P < 0.001$ indicate significant differences compared to the control group; $^{*}P < 0.05$, $^{**}P < 0.01$, and $^{***}P < 0.001$ versus CSE group. SIRT1, Silent information regulator 1; NF-κB, nuclear factor kappaB; TNF-α, tumor necrosis factor alpha; IL, interleukin; SFN, sulforaphane; CSE, cigarette smoke extract; qRT-PCR, quantitative real-time polymerase chain reaction; GAPDH, glyceraldehyde-3-phosphate dehydrogenase.

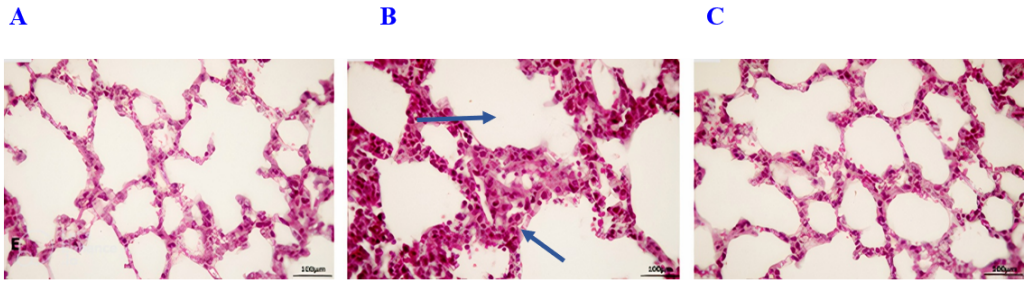

Fig. 6. Representative H&E-stained lung tissues of mice (scale bars, 100 µm and 200 µm). (A) Control group, (B) CSE group, and (C) CSE + SFN-treated group. Arrows indicate alveolar destruction and enlarged airspaces characteristic of emphysematous changes. SFN, sulforaphane; CSE, cigarette smoke extract; H&E, hematoxylin and eosin.

SFN protects against CSE-induced lung damage in a COPD mouse model

An emphysema model was established in six-week-old mice through intraperitoneal administration of liquid CSE. H&E staining was performed to assess lung histopathology (Fig. 6). As shown in Fig. 6B, lung sections from the CSE-treated group exhibited marked thickening of the alveolar walls due to inflammatory cell infiltration, along with the formation of enlarged air spaces and pronounced emphysematous changes, which are characteristic histopathological features of COPD. In contrast, co-treatment with SFN significantly mitigated these pathological alterations, as evidenced by a reduction in alveolar wall thickening and inflammatory infiltration, thereby preserving lung architecture (Fig. 6C). Also, to provide semi-quantitative support for the observed emphysematous changes, the mean linear intercept (MLI) was calculated based on H&E-stained images. The MLI significantly increased

in the CSE group (2.16 μm) compared to the control group (1.80 μm), indicating alveolar enlargement. Treatment with SFN reduced the MLI to 1.71 μm, suggesting a protective effect against CSE-induced alveolar destruction. These results indicate that SFN may play a protective role in mitigating pulmonary injury caused by exposure to CSE.

DISCUSSION

This study presents compelling evidence supporting the protective capacity of SFN against CSE-induced cellular damage, primarily through the suppression of oxidative stress, ferroptosis, and cellular senescence in both *in vitro* and *in vivo* models. Given their role as the frontline defense against inhaled environmental insults, airway epithelial cells are particularly critical in mediating these protective effects (33). Both *in vitro* and *in vivo* studies have demonstrated that exposure to CS is sufficient to induce cellular senescence, oxidative stress, and ferroptosis (5,17,34). Notably, SFN has been shown to exert protective effects by activating SIRT1, which plays a crucial role in regulating oxidative stress responses, cellular senescence, and inflammation (35). In agreement with previous findings (36,37), CSE exposure in our study induced significant cytotoxicity and reduced cell viability. Notably, co-treatment with SFN at 10 μg/mL efficiently ameliorated this toxicity, confirming its cytoprotective potential. Importantly, we used CSE at IC_{50} in combination with moderate doses of SFN to evaluate therapeutic relevance while avoiding overwhelming cytotoxicity that might mask potential protective effects. These dose combinations were selected based on initial dose-response data and are consistent with concentrations used in prior studies investigating SFN's protective roles. Our results further corroborate previous reports of oxidative stress induced by cigarette smoke, as evidenced by elevated ROS and reduced intracellular GSH levels. This oxidative imbalance is known to contribute not only to cellular damage but also to the initiation of senescence and ferroptosis (38-40). SFN effectively restored antioxidant capacity by enhancing GSH levels and reducing ROS, reinforcing its antioxidative function.

Oxidative stress induced by CS is closely linked to cellular senescence through multiple mechanisms (41). Senescent cells are characterized by increased expression of β-galactosidase, an enzyme detectable at pH 6, commonly referred to as SA-β-gal, which serves as a widely used biomarker for senescence. A key mechanism through which cells sustain the senescent state involves the modulation of senescence-associated gene expression, including the upregulation of genes such as p16 and p21. In the present study, treatment with CSE led to a significant elevation in the proportion of SA-β-gal-positive BEAS-2B cells, accompanied by upregulated expression of the senescence-associated markers p16 and p21. Additionally, CSE exposure enhanced the secretion of SASP cytokines, including IL-6, IL-1β, TNF-α, and IL-8, further supporting the role of CSE in promoting cellular senescence in airway epithelial cells. Notably, SFN at a concentration of 10 μg/mL effectively reduced these senescence markers, demonstrating its potential anti-senescence properties.

SIRT1 is a protein crucial for cellular function and regulates various cellular processes (42). Our findings revealed that exposure to CSE led to a marked downregulation of SIRT1 mRNA expression, accompanied by an upregulation of NF-κB and its downstream pro-inflammatory cytokines, including IL-8, TNF-α, and IL-6. Previous studies have shown that SIRT1 can interact directly with the RelA/p65 subunit of NF-κB, suppressing its transcriptional activity through deacetylation mechanisms (43,44). The observed downregulation of SIRT1 and concurrent upregulation of NF-κB in response to CSE exposure suggest that CS promotes inflammation and senescence *via* SIRT1 suppression. We selected SFN for this study because of its well-documented ability to activate SIRT1 and inhibit inflammatory pathways, including NF-κB signaling. SFN's modulatory effects on oxidative stress and inflammation are particularly relevant in the context of CS-induced cellular damage, where oxidative stress, inflammation, and senescence converge as interconnected mechanisms driving COPD pathogenesis (45,46). Importantly, SFN's activation of SIRT1 may synergize with its antioxidant function to form a dual mechanism of

protection. Through SIRT1-mediated NF-κB inhibition and redox balance restoration, SFN appears to break the positive feedback loop between inflammation and oxidative damage. This dual mechanism may explain the superior efficacy of combination treatment (CSE + SFN) compared to CSE exposure alone, highlighting a potential therapeutic strategy.

Histopathological analysis further supports the protective role of SFN against CSE-induced lung damage. Our study established an emphysema model in mice *via* intraperitoneal administration of liquid CSE, leading to significant structural alterations in lung tissue. H&E staining revealed marked alveolar wall thickening due to inflammatory cell infiltration, enlarged air spaces, and emphysematous changes-hallmark histopathological features of COPD. These observations align with earlier studies indicating that prolonged exposure to CS triggers sustained inflammatory responses and contributes to progressive structural deterioration of lung tissue (47,48). Notably, SFN co-treatment effectively mitigated these pathological changes by reducing alveolar wall thickening and inflammatory infiltration, thereby preserving lung architecture. These results imply that SFN may confer protective benefits to lung tissue by regulating inflammatory responses and oxidative stress, thereby potentially inhibiting or slowing the development of emphysematous alteration.

Ferroptosis, a regulated form of cell death characterized by iron overload and excessive lipid peroxidation, has emerged as a key contributor to cellular injury induced by CSE (13). The present study demonstrated that exposure to CSE leads to a substantial increase in intracellular iron concentration and MDA levels, both hallmarks of ferroptotic cell death. The elevation in iron levels suggests that CSE disrupts iron homeostasis, thereby promoting oxidative stress and lipid peroxidation, which are key contributors to ferroptosis. SFN treatment was effective in mitigating ferroptosis by significantly reducing iron accumulation and lipid peroxidation. The observed decrease in MDA levels following SFN treatment further supports its protective role against ferroptosis. DFO (an iron chelator), by chelating free Fe^{2+} ions, significantly inhibits the ferroptosis pathway through the reduction of lipid peroxidation, while also mitigating general oxidative stress mechanisms by decreasing ROS production. This aligns with previous findings suggesting that SFN enhances antioxidant defenses and iron metabolism regulation, thereby counteracting ferroptotic processes (49). To explore the molecular basis of SFN's protective action, we assessed the expression levels of pivotal genes associated with ferroptosis, specifically SLC7A11 and GPX4. SLC7A11 functions as a vital subunit of the cystine/glutamate antiporter (System Xc^-), which plays an essential role in preserving intracellular GSH concentrations and mitigating lipid peroxidation (50). GPX4, an important regulator of ferroptosis, mitigates lipid peroxidation by converting lipid hydroperoxides into non-toxic lipid alcohols (16). Since GPX4 activity depends on the availability of GSH, its reduction in CSE-treated cells may further exacerbate lipid peroxidation, thereby promoting ferroptosis. Our results demonstrated that CSE exposure led to the downregulation of GPX4 and SLC7A11, impairing cellular antioxidant defenses and promoting ferroptosis. However, SFN treatment restored SLC7A11 and GPX4 expression, suggesting its role in enhancing cellular resilience against CSE-induced ferroptotic damage. Although DFO reduced iron accumulation, it did not fully prevent MDA elevation, suggesting that ferroptosis is not the sole contributor to lipid peroxidation and that oxidative stress *via* other pathways also plays a role. This observation highlights the complexity of cell death mechanisms under CS exposure and the multifaceted action of SFN. Together, these findings suggest that SFN mediates its protective effects through multiple intersecting molecular pathways: enhancing antioxidant defenses (via GSH and ROS reduction), suppressing ferroptosis (through upregulation of GPX4/SLC7A11 and iron homeostasis), and attenuating inflammation and senescence (*via* SIRT1 activation and NF-κB inhibition). These results suggest that SFN may serve as a potential therapeutic agent by targeting key mechanisms such as oxidative stress, inflammation, cellular senescence, and ferroptosis to prevent or reduce COPD progression in smokers by targeting key pathogenic mechanisms.

Despite the promising findings, this study has a main limitation. The *in vitro* concentrations of

SFN may not directly translate to physiological levels achievable through dietary intake, although pharmacological relevance has been supported by previous studies. For instance, Clarke *et al.* reported that SFN plasma levels after consumption of broccoli sprout extracts are significantly lower than the concentrations used in cellular assays; however, such models are essential for understanding underlying mechanisms and guiding the development of concentrated supplements or therapeutic formulations (51). Future studies should focus on *in vivo* validation of these findings, dose optimization, and the evaluation of SFN's efficacy in animal models or clinical settings to better assess its translational potential.

CONCLUSION

In conclusion, this study identified SFN as a promising phytochemical capable of mitigating the toxic effects of CSE. SFN exhibited notable anti-inflammatory, anti-ferroptotic, and anti-senescent properties. Mechanistically, these protective effects were strongly associated with the restoration of SIRT1 expression, a key regulator of oxidative stress and inflammation. By upregulating SIRT1, SFN effectively suppressed NF-κB activity and reduced the expression of its downstream pro-inflammatory cytokines, thereby attenuating CSE-induced cellular damage. While these findings are encouraging, further investigations, including a detailed exploration of cellular mechanisms, are warranted to confirm and expand upon these results.

Acknowledgments

The authors thank Milad Chahardori from the Student Research Committee, Faculty of Pharmacy, Mazandaran University of Medical Sciences, Sari, Iran, for his help and advice.

This research was financially supported by Mazandaran University of Medical Sciences in Sari, Iran, through Grant No. 18270 and ethical approval code IR.MAZUMS.AEC.1403.043.

Conflict of interest statement

The authors declared that they have no financial conflicts of interest or personal affiliations that could have influenced the objectivity or integrity of the results presented in this article.

Authors' contributions

A. Reihani performed all tests in the study, wrote the original draft, analyzed the data, reviewed, and revised the article; E. Mohammadi supervised the molecular tests and reviewed the manuscript; M. Seyedabadi contributed to the conceptualization, methodology, supervision, and investigation; F. Talebpour Amiri performed histophatology analysis; F. Shaki contributed to conceptualization, supervision, review and editing the article. All authors read and approved the final version. As stated earlier in this document, the requirements for authorship have been met. Each author believes that the manuscript represents honest work

Data availability

The data generated in our research are available upon request from the corresponding author.

REFERENCES

1. Smith CJ, Hansch C. The relative toxicity of compounds in mainstream cigarette smoke condensate. Food Chem Toxicol. 2000;38(7):637-46. DOI: 10.1016/s0278-6915(00)00051-x.
2. Patel RR, Ryu JH, Vassallo R. Cigarette smoking and diffuse lung disease. Drugs. 2008;68(11):1511-1527. DOI: 10.2165/00003495-200868110-00004.
3. Zeng XL, Yang XN, Liu XJ. Resveratrol attenuates cigarette smoke extract induced cellular senescence in human airway epithelial cells by regulating the miR-34a/SIRT1/NF-κB pathway.Medicine. 2022;101(46):e31944,1-8. DOI:10.1097/md.0000000000031944.
4. Yang SR, Wright J, Bauter M, Seweryniak K, Kode A, Rahman I. Sirtuin regulates cigarette smoke-induced proinflammatory mediator release via RelA/p65 NF-κB in macrophages *in vitro* and in rat lungs *in vivo*:implications for chronic inflammation and aging. Am J Physiol Lung Cell Mol Physiol.2007;292(2):L567-L576. DOI: 10.1152/ajplung.00308.2006.
5. Satrialdi, Pratiwi C, Khaeranny RN, Mudhakir D. The development of mitochondria-targeted quercetin for rescuing Sertoli cells from oxidative stress. Res Pharm Sci. 2025;20(1):109-120. DOI: 10.4103/RPS.RPS_226_23.
6. Ma N, Deng TT, Wang Q, Luo ZL, Zhu CF, Qiu JF, *et al.* Erythromycin regulates cigarette smoke-induced proinflammatory mediator release through

sirtuin 1-nuclear factor κB axis in macrophages and mice lungs. Pathobiology. 2019;86(5-6):237-247. DOI: 10.1159/000500628.
7. Barnes PJ. Senescence in COPD and its comorbidities. Annu Rev Physiol. 2017;79:517-639. DOI: 10.1146/annurev-physiol-022516-034314.
8. Zhang Y, Huang W, Zheng Z, Wang W, Yuan Y, Hong Q, *et al*. Cigarette smoke-inactivated SIRT1 promotes autophagy-dependent senescence of alveolar epithelial type 2 cells to induce pulmonary fibrosis. Free Radic Biol Med. 2021;166:116-127. DOI: 10.1016/j.freeradbiomed.2021.02.013.
9. Easter M, Bollenbecker S, Barnes JW, Krick S. Targeting aging pathways in chronic obstructive pulmonary disease. Int J Mol Sci. 2020;21(18):6924,1-17. DOI: 10.3390/ijms21186924.
10. Campisi J. Aging, cellular senescence, and cancer. Annu Rev Physiol. 2013;75:685-705. DOI: 10.1146/annurev-physiol-030212-183653.
11. González-Gualda E, Baker AG, Fruk L, Muñoz-Espín D. A guide to assessing cellular senescence *in vitro* and *in vivo*. FEBS. 2021;288(1):56-80. DOI: 10.1111/febs.15570.
12. van Deursen JM. The role of senescent cells in ageing. Nature. 2014;509(7501):439-446. DOI: 10.1038/nature13193.
13. Du Y, Ding Y, Shi T, He W, Mei Z, Feng X, *et al*. Suppression of circXPO1 attenuates cigarette smoke-induced inflammation and cellular senescence of alveolar epithelial cells in chronic obstructive pulmonary disease. Int Immunopharmacol. 2022;111:109086. DOI: 10.1016/j.intimp.2022.109086.
14. Xia H, Wu Y, Zhao J, Cheng C, Lin J, Yang Y, *et al*. N6-Methyladenosine-modified circSAV1 triggers ferroptosis in COPD through recruiting YTHDF1 to facilitate the translation of IREB2. Cell Death Differ. 2023;30(5):1293-1304. DOI: 10.1038/s41418-023-01138-9.
15. Feng L, Sun J, Xia L, Shi Q, Hou Y, Zhang L, *et al*. Ferroptosis mechanism and Alzheimer's disease. Neural Regen Res. 2024;19(8):1741-1750. DOI: 10.4103/1673-5374.389362.
16. Chen X, Li J, Kang R, Klionsky DJ, Tang D. Ferroptosis:machinery and regulation. Autophagy. 2021;17(9):2054-2081. DOI: 10.1080/15548627.2020.1810918.
17. Riegman M, Sagie L, Galed C, Levin T, Steinberg N, Dixon SJ, *et al*. Ferroptosis occurs through an osmotic mechanism and propagates independently of cell rupture. Nat Cell Biol. 2020;22(9):1042-1048. DOI: 10.1038/s41556-020-0565-1.
18. Chen J, Deng X, Xie H, Wang C, Huang J, Lian N. Circular RNA_0025843 alleviated cigarette smoke extract induced bronchoalveolar epithelial cells ferroptosis. Int J Chron Obstruct Pulmon Dis. 2024;19:363-374. DOI: 10.2147/copd.s444402.
19. Haigis MC, Sinclair DA. Mammalian sirtuins:biological insights and disease relevance. Annu Rev Pathol. 2010;5(1):253-295. DOI: 10.1146/annurev.pathol.4.110807.092250.
20. Hall JA, Dominy JE, Lee Y, Puigserver P. The sirtuin family's role in aging and age-associated pathologies. J Clin Invest. 2013;123(3):973-979. DOI: 10.1172/JCI64094.
21. Yao H, Sundar IK, Ahmad T, Lerner C, Gerloff J, Friedman AE, *et al*. SIRT1 protects against cigarette smoke-induced lung oxidative stress via a FOXO3-dependent mechanism. Am J Physiol Lung Cell Mol. 2014;306(9):L816-L28. DOI: 10.1152/ajplung.00323.2013.
22. Ebrahim NA, Elnagar MR, El-Gamal R, Habotta OA, Albadawi EA, Albadrani M, *et al*. Melatonin mitigates doxorubicin induced chemo brain in a rat model in a NRF2/p53-SIRT1 dependent pathway. Heliyon. 2024;10(19):e38081,1-15. DOI:10.1016/j.heliyon.2024.e38081.
23. Guarente L. Sirtuins, aging, and medicine. N Engl J Med. 2011;364(23):2235-2244. DOI: 10.1056/NEJMra1100831.
24. Biswas S, W Hwang J, A Kirkham P, Rahman I. Pharmacological and dietary antioxidant therapies for chronic obstructive pulmonary disease. Curr Med Chem. 2013;20(12):1496-1530. DOI: 10.2174/0929867311320120004.
25. Danilov CA, Chandrasekaran K, Racz J, Soane L, Zielke C, Fiskum G. Sulforaphane protects astrocytes against oxidative stress and delayed death caused by oxygen and glucose deprivation. Glia. 2009;57(6):645-656. DOI: 10.1002/glia.20793.
26. Juge N, Mithen RF, Traka M. Molecular basis for chemoprevention by sulforaphane:a comprehensive review. Cell. Mol Life Sci. 2007;64(9):1105-1127. DOI: 10.1007/s00018-007-6484-5.
27. Ping Z, Liu W, Kang Z, Cai J, Wang Q, Cheng N, *et al*. Sulforaphane protects brains against hypoxic-ischemic injury through induction of Nrf2-dependent phase 2 enzyme. Brain Res. 2010;1343:178-185. DOI: 10.1016/j.brainres.2010.04.036.
28. Zhang Y, Cao J, Chen Y, Chen P, Peng H, Cai S, *et al*. Intraperitoneal injection of cigarette smoke extract induced emphysema, and injury of cardiac and skeletal muscles in BALB/C mice. Exp Lung Res. 2013;39(1):18-31. DOI: 10.3109/01902148.2012.745910.
29. Reihani A, Shaki F, Azari A. Zinc oxide nanoparticles decrease acrylamide cytotoxicity and oxidative stress in HepG2 cells. Curr Res Nutr Food Sci. 2025;55(3):481-492. DOI: 10.1108/NFS-07-2023-0147.
30. Zhao Z, Xu Z, Chang J, He L, Zhang Z, Song X, et al. Sodium pyruvate exerts protective effects against cigarette smoke extract-induced ferroptosis in alveolar and bronchial epithelial cells through the GPX4/Nrf2 axis. J Inflamm. 2023;20(1):28,1-11. DOI: 10.1186/s12950-023-00347-w.

31. Uchil PD, Nagarajan A, Kumar P. Assay for β-galactosidase in extracts of mammalian cells. Cold Spring Harb Protoc. 2017;2017(10):837-841. DOI: 10.1101/pdb.prot095778.
32. Jiao Z, Chang J, Li J, Nie D, Cui H, Guo D. Sulforaphane increases Nrf2 expression and protects alveolar epithelial cells against injury caused by cigarette smoke extract. Mol Med Rep. 2017;16(2):1241-1247. DOI: 10.3892/mmr.2017.6700.
33. Livak KJ, Schmittgen TD. Analysis of relative gene expression data using real-time quantitative PCR and the 2(-Delta Delta C(T)) Method. Methods. 2001;25(4):402-408. DOI:10.1006/meth.2001.1262.
34. Jalili C, Korani M, Pazhouhi M, Ghanbari A, Zhaleh M, Davoudi S, *et al*. Protective effect of gallic acid on nicotine-induced testicular toxicity in mice. Res Pharm Sci. 2021;16(4):414-424. DOI: 10.4103/1735-5362.319579.
35. Chiaradia E, Sansone A, Ferreri C, Tancini B, Latella R Tognoloni A, *et al*. phospholipid fatty acid remodeling and carbonylated protein increase in extracellular vesicles released by airway epithelial cells exposed to cigarette smoke extract. Eur J Cell Biol. 2023;102(1):151285,1-11. DOI: 10.1016/j.ejcb.2022.151285.
36. Guo P, Pi H, Xu S, Zhang L, Li Y, Li M, *et al*. Melatonin improves mitochondrial function by promoting MT1/SIRT1/PGC-1 alpha-dependent mitochondrial biogenesis in cadmium-induced hepatotoxicity *in vitro*. Toxicol Sci. 2014;142(1):182-195. DOI: 10.1093/toxsci/kfu164.
37. Bendary MM, Ali MAM, Abdel Halim AS, Boufahja F, Chaudhary AA, Elkelish A, *et al*. Investigating Sulforaphane's anti-virulence and anti-quorum sensing properties against *Pseudomonas aeruginosa*. Front Pharmacol. 2024;15:1406653,1-21. DOI:10.3389/fphar.2024.1406653.
38. Yasuda S, Horinaka M, Sakai T. Sulforaphane enhances apoptosis induced by *Lactobacillus pentosus* strain S-PT84 via the TNFα pathway in human colon cancer cells. Oncol Lett. 2019;18(4):4253-4261. DOI: 10.3892/ol.2019.10739.
39. Rajaei N, Rahgouy G, Panahi N, Razzaghi-Asl N. Bioinformatic analysis of highly consumed phytochemicals as P-gp binders to overcome drug-resistance. Res Pharm Sci. 2023;18(5): 505-516. DOI: 10.4103/1735-5362.383706.
40. Zanichelli F, Capasso S, Cipollaro M, Pagnotta E, Cartenì M, Casale F, *et al*. Dose-dependent effects of R-sulforaphane isothiocyanate on the biology of human mesenchymal stem cells, at dietary amounts, it promotes cell proliferation and reduces senescence and apoptosis, while at anti-cancer drug doses, it has a cytotoxic effect. Age (Dordrecht, Netherlands). 2012;34(2):281-293. DOI: 10.1007/s11357-011-9231-7.
41. Jackson SJ, Singletary KW. Sulforaphane inhibits human MCF-7 mammary cancer cell mitotic progression and tubulin polymerization. J Nutr. 2004;134(9):2229-2236. DOI: 10.1093/jn/134.9.2229.
42. Wu H, Ma H, Wang L, Zhang H, Lu L, Xiao T, *et al*. Regulation of lung epithelial cell senescence in smoking-induced COPD/emphysema by microR-125a-5p via Sp1 mediation of SIRT1/HIF-1a. Int J Biol Sci. 2022;18(2):661-674. DOI: 10.7150/ijbs.65861.
43. Karakuyu NF, Özseven A, Akın SE, Çamaş HE, Özmen Ö, Cengiz Ç. L-carnitine protects the lung from radiation-induced damage in rats via the AMPK/SIRT1/TGF-1ß pathway. Naunyn Schmiedebergs Arch Pharmacol. 2024;397(10):8043-8051. DOI: 10.1007/s00210-024-03157-w.
44. Yeung F, Hoberg JE, Ramsey CS, Keller MD, Jones DR, Frye RA, *et al*. Modulation of NF-kappaB-dependent transcription and cell survival by the SIRT1 deacetylase. EMBO J. 2004;23(12):2369-23480. DOI: 10.1038/sj.emboj.7600244.
45. Deng M, Tong R, Bian Y, Hou G. Astaxanthin attenuates cigarette smoking-induced oxidative stress and inflammation in a sirtuin 1-dependent manner. Biomed Pharmacother. 2023;159:114230,1-14. DOI: 10.1016/j.biopha.2023.114230.
46. Chen W, Sun Z, Wang XJ, Jiang T, Huang Z, Fang D, *et al*. Direct interaction between Nrf2 and p21(Cip1/WAF1) upregulates the Nrf2-mediated antioxidant response. Mol Cell. 2009;34(6):663-673. DOI: 10.1016/j.molcel.2009.04.029.
47. Kubo E, Chhunchha B, Singh P, Sasaki H, Singh DP. Sulforaphane reactivates cellular antioxidant defense by inducing Nrf2/ARE/Prdx6 activity during aging and oxidative stress. Sci Rep. 2017;7(1):14130,1-17. DOI: 10.1038/s41598-017-14520-8.
48. Yu Z, He W, Shi W. Sulforaphane (Sul) reduces renal interstitial fibrosis (RIF) by controlling the inflammation and TGF-β/Smad signaling pathway. Appl Biol Chem. 2024;67(1):8,1-11. DOI: 10.1186/s13765-024-00858-x.
49. Pogorzelska A, Świtalska M, Wietrzyk J, Mazur M, Milczarek M, Medyńska K, *et al*. Antitumor and antimetastatic effects of dietary sulforaphane in a triple-negative breast cancer models. Sci Rep. 2024;14(1):16016,1-11. DOI: 10.1038/s41598-024-65455-w.
50. Yan M, Xu S, Wang H, Dong S, Mo C. Ferroptosis in chronic obstructive pulmonary disease:from cellular mechanisms to therapeutic applications. Chin Med J. 2024;137(10):1237-1239. DOI: 10.1097/cm9.0000000000003079.
51. Terzi EM, Sviderskiy VO, Alvarez SW, Whiten GC, Possemato R. Iron-sulfur cluster deficiency can be sensed by IRP2 and regulates iron homeostasis and sensitivity to ferroptosis independent of IRP1 and FBXL5. Sci Adv. 2021;7(22):1-11. DOI: 10.1126/sciadv.abg4302.